

Geochemistry, Geophysics, Geosystems



RESEARCH ARTICLE

10.1029/2024GC011594

Key Points:

- Magnetic microscopy can be used to produce a 5× improvement in temporal resolution of magnetic records from speleothems
- Variations in magnetic properties across speleothems can affect the temporal resolution of the magnetic record
- Protocols for conducting highresolution magnetic measurements of speleothems with magnetic microscopy are presented

Correspondence to:

C. S. Borlina, cborlina@purdue.edu

Citation

Borlina, C. S., Lima, E. A., Feinberg, J. M., Jaqueto, P., Lascu, I., Trindade, R. I. F., et al. (2024). Obtaining high-resolution magnetic records from speleothems using magnetic microscopy. *Geochemistry*, *Geophysics, Geosystems*, 25, e2024GC011594. https://doi.org/10.1029/2024GC011594

Received 3 APR 2024 Accepted 18 JUL 2024

Author Contributions:

Conceptualization: Cauê S. Borlina, Eduardo A. Lima, Joshua M. Feinberg Data curation: Cauê S. Borlina, Eduardo A. Lima

Formal analysis: Cauê S. Borlina, Eduardo A. Lima

Funding acquisition: Eduardo A. Lima, Joshua M. Feinberg, Ioan Lascu, Benjamin P. Weiss

Investigation: Cauê S. Borlina, Eduardo A. Lima, Plinio Jaqueto, Ioan Lascu, Ricardo I. F. Trindade, Eric Font, Luca Antonio Dimuccio, Yusuke Yokoyama, Josep M. Parés, Benjamin P. Weiss Methodology: Cauê S. Borlina, Eduardo A. Lima, Joshua M. Feinberg

© 2024 The Author(s). Geochemistry, Geophysics, Geosystems published by Wiley Periodicals LLC on behalf of American Geophysical Union.
This is an open access article under the terms of the Creative Commons
Attribution-NonCommercial-NoDerivs
License, which permits use and distribution in any medium, provided the original work is properly cited, the use is non-commercial and no modifications or adaptations are made.

Obtaining High-Resolution Magnetic Records From Speleothems Using Magnetic Microscopy

Cauê S. Borlina^{1,2,3}, Eduardo A. Lima³, Joshua M. Feinberg⁴, Plinio Jaqueto⁴, Ioan Lascu⁵, Ricardo I. F. Trindade⁶, Eric Font⁷, Elisa M. Sánchez-Moreno⁸, Luca Antonio Dimuccio⁹, Yusuke Yokoyama¹⁰, Josep M. Parés¹¹, Benjamin P. Weiss³, and Jeffrey A. Dorale¹²

¹Department of Earth, Atmospheric, and Planetary Sciences, Purdue University, West Lafayette, IN, USA, ²Department of Earth and Planetary Sciences, Johns Hopkins University, Baltimore, MD, USA, ³Department of Earth, Atmospheric and Planetary Sciences, Massachusetts Institute of Technology, Cambridge, MA, USA, ⁴Department of Earth and Environmental Sciences, Institute for Rock Magnetism, University of Minnesota, Minneapolis, MN, USA, ⁵Department of Mineral Sciences, National Museum of Natural History, Smithsonian Institution, Washington, DC, USA, ⁶Instituto de Astronomia, Geofísica e Ciências Atmosféricas, Universidade de São Paulo, São Paulo, Brazil, ⁷Departamento de Ciências da Terra, Universidade de Coimbra, Coimbra, Portugal, ⁸Departamento de Física, EPS, Universidade de Burgos, Burgos, Spain, ⁹University of Coimbra, Centre of Studies in Geography and Spatial Planning (CEGOT), Coimbra, Portugal, ¹⁰Atmosphere and Ocean Research Institute, The University of Tokyo, Bunkyo City, Japan, ¹¹Centro Nacional de Investigación sobre la Evolución Humana, Burgos, Spain, ¹²Department of Earth and Environmental Sciences, University of Iowa, Iowa, IA, USA

Abstract Speleothems are mineral deposits capable of recording detrital and/or chemical remanent magnetization at annual timescales. They can offer high-resolution paleomagnetic records of short-term variations in Earth's magnetic field, crucial for understanding the evolution of the dynamo. Owing to limitations on the magnetic moment sensitivity of commercial cryogenic rock magnetometers (~10⁻¹¹ Am²), paleomagnetic studies of speleothems have been limited to samples with volumes of several hundreds of mm³, averaging tens to hundreds of years of magnetic variation. Nonetheless, smaller samples (~1-10 mm³) can be measured using superconducting quantum interference device (SQUID) microscopy, with a sensitivity better than $\sim 10^{-15}$ Am². To determine the application of SQUID microscopy for obtaining robust high-resolution records from small-volume speleothem samples, we analyzed three different stalagmites collected from Lapa dos Morcegos Cave (Portugal), Pau d'Alho Cave (Brazil), and Crevice Cave (United States). These stalagmites are representative of a range of magnetic properties and have been previously studied with conventional rock magnetometers. We show that by using SQUID microscopy we can achieve a five-fold improvement in temporal resolution for samples with higher abundances of magnetic carriers (e.g., Pau d'Alho Cave and Lapa dos Morcegos Cave). In contrast, speleothems with low abundances of magnetic carriers (e.g., Crevice Cave) do not benefit from higher resolution analysis and are best analyzed using conventional rock magnetometers. Overall, by targeting speleothem samples with high concentrations of magnetic carriers we can increase the temporal resolution of magnetic records, setting the stage for resolving geomagnetic variations at short time scales.

Plain Language Summary Earth has a magnetic field that is generated in the outer core, and through paleomagnetism we can retrieve information about the evolution of the field from rocks. Different types of rocks have been used to determine how Earth's magnetic field has changed over time. In this study, we use magnetic microscopy to analyze the magnetic record of speleothems, which are rocks that form inside caves and that can record magnetic fields in annual scales. This allows us to obtain magnetic records with higher resolution than previous studies. This is important because Earth's magnetic field changes in timescales ranging from thousands of years to a few years, and obtaining records from speleothems using magnetic microscopy can help us track these variations. We provide data demonstrating how the technique can be used and showing its limitations, and we discuss how the geologic context of the cave influences the robustness of the magnetic record. We also provide protocols for future studies using magnetic microscopy in speleothems.

1. Introduction

Speleothems are mineral deposits formed in caves by dripping, pooling, or seeping water containing dissolved ions and mineral grains from the host bedrock and overlying soils. Because speleothems typically precipitate at

BORLINA ET AL. 1 of 20

8 ' O ;;; N6 ' ?;; N O ; -N9
?; -N ?;; 4: '
; ' 8 O ; -:?

' D) ' A K" " E

'

wiley.com/doi/10.1029/2024GC011594 by University Of Minnesota Lib, Wiley Online Library on [13/11/2024]. See the Term

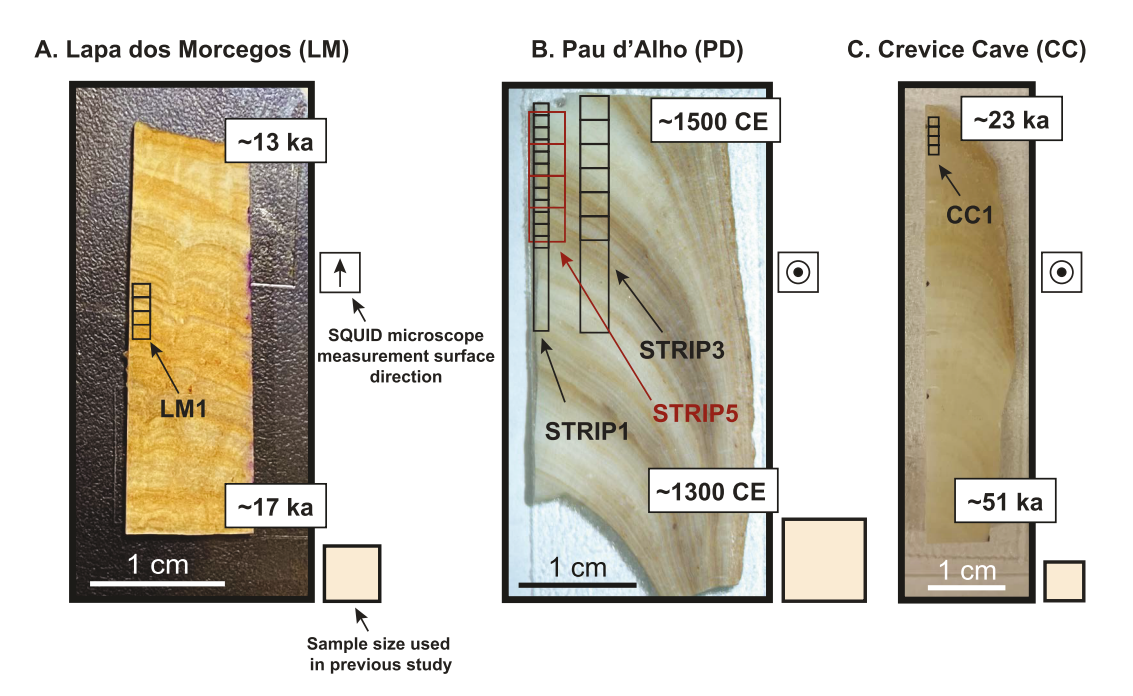


Figure 1. *Images of the speleothems analyzed in this study.* Shown are the thick sections along with the longitudinal strips extracted from speleothems from (a) Lapa dos Morcegos Cave, (b) Pau d'Alho Cave and (c) Crevice Cave. The squares across the longitudinal strips indicate how the samples were cut. The boxes on the lower right side of each sample show the approximate size of the samples used in previous paleomagnetic measurements of the samples. The box to the center right indicate the direction of the surface used to obtain the superconducting quantum interference device (SQUID) microscope magnetic maps.

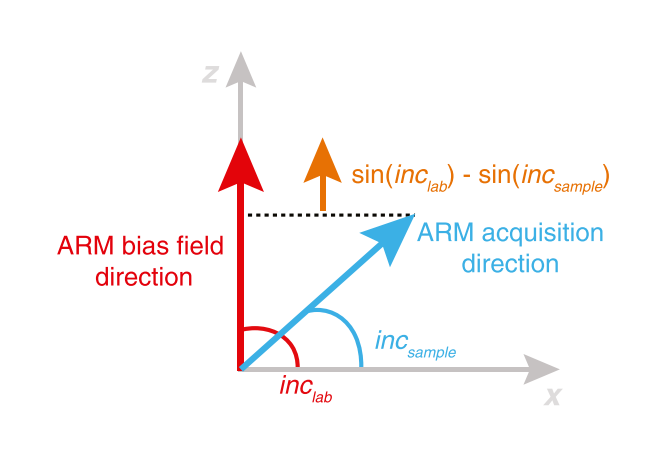
Second, we analyzed a speleothem from the Pau d'Alho Cave System, Brazil (henceforth identified as PD). Previous work by Trindade et al. (2018) studied two speleothems (ALHO 06 and ALHO 31), which have overlapping magnetic records from the last ~1,600 years. These speleothems are mainly composed of calcite, with a complete mineralogical description found in Jaqueto et al. (2016). ALHO 31 was oriented in situ with a magnetic compass, while ALHO 06 had its orientation estimated by matching its declination record to field models for the same age interval. Ages for the PD samples were obtained using the U-Th method and layer counting (Novello et al., 2016; Trindade et al., 2018). We focused on a section from ALHO 06 that was available from the previous study and contained magnetic records between the years 1500 and 1600 CE (Figure 1b). Trindade et al. (2018) measured samples with a thickness of ~7 mm and a total volume of ~1,900 mm³, which corresponds to averaging about 45 years of magnetic field variation.

Third, we studied a stalagmite from Crevice Cave, Missouri, United States (henceforth identified as CC). This speleothem was previously analyzed by Lascu et al. (2016) and provided records of the Laschamp excursion. The speleothem was originally collected for climate studies and was not oriented in the field. The total speleothem length was \sim 20 cm and contained magnetic records between 65 and 25 thousands of years (ka) ago (Figure 1c). Ages were obtained using the U-Th method and annual layer counting was anchored to the U-Th age depth curve. Lascu et al. (2016) analyzed samples with a thickness of 4–5 mm and a total volume of \sim 595 mm³ that corresponded to averaging approximately one thousand years of magnetic field variation. Given that all three samples were previously studied using superconducting rock magnetometers, the measurements in this study were carried out on speleothem sections adjacent to the central part used in those studies, with varying degrees of layer curvature present. We discuss later the potential effects of the curvature to the magnetic record of a speleothem sample.

2.2. Sample Preparation

We prepared our samples in the Massachusetts Institute of Technology (MIT) Paleomagnetism Laboratory inside a positive-pressure shielded room to minimize contamination (field <200 nT). Samples were cut using a precision diamond wire saw (0.2 mm diameter wire) with deionized water as a cooling fluid.

BORLINA ET AL. 3 of 20



?& : C ?& S

6 ((

;;

6) ?B ?:) ; 35 ?& ; 25@):?6

& %8% @ : 86 ' :?6 & , 8 , 4@ ,:?& ? 8 ?B ?: -% 8 %? B %?:

8,?B,?:? 86' 8((? B((?:)

)@ ?8; : ?6 , B ; R) Е 3

? ; :?& 3 ? (' ?8;;4:) 9 E ??8 ; ; 7:

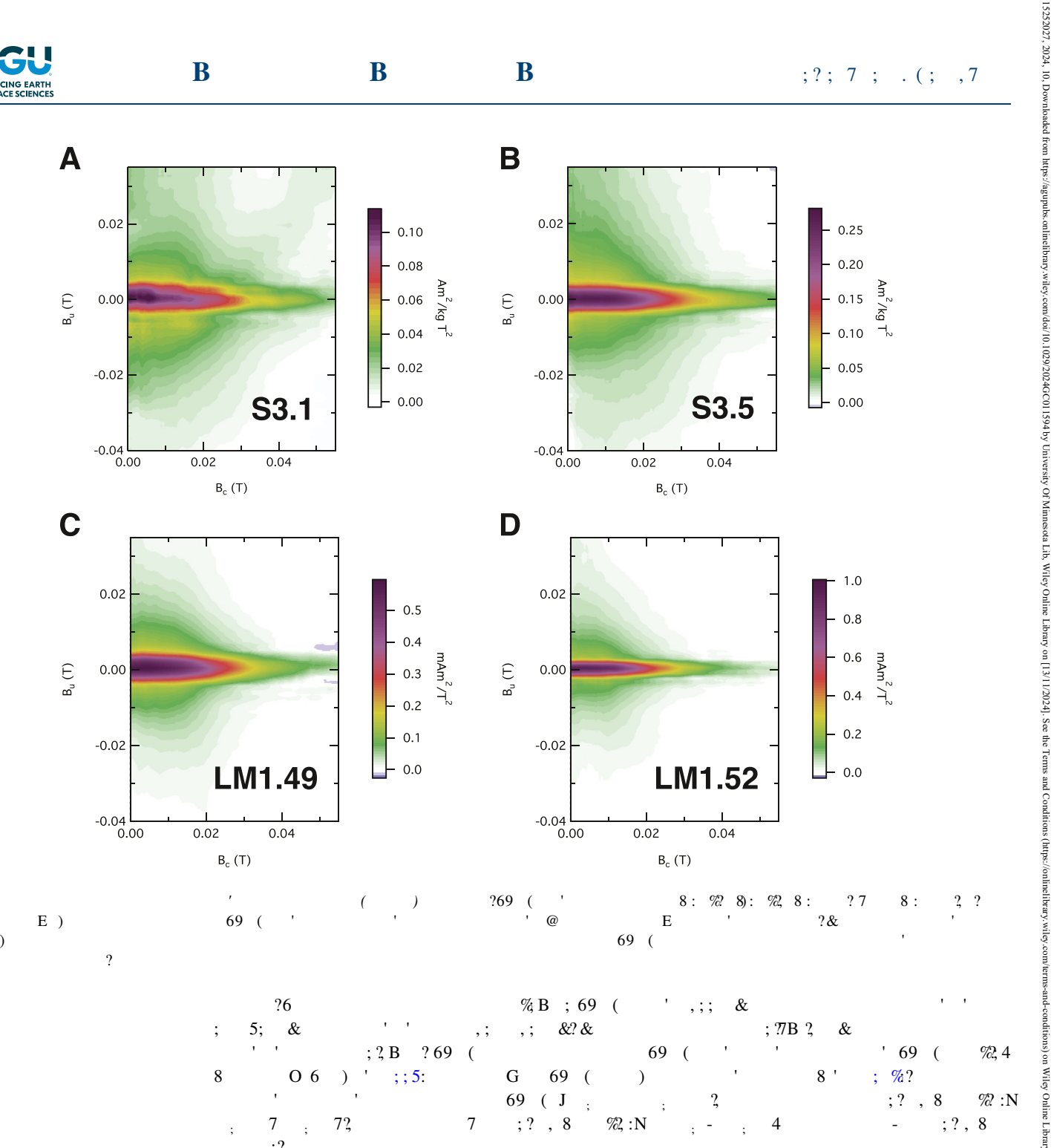
5) 869 (: E) % 8 %? ' 5-; , :?69 (%? %2,) (**G**)

8 : ' %; & ; ; *&*?*&* & ' %7;; G) ' **%?** ?69 (? 7 ?

8L "

3

8 7



3 8 :) ' '@E ' 8 6: ?6 & ?8; 5:) "
?8; -:?

8 ?;;5:? 6 ' 3) " ((,; &? ' D

3@

& ?

A

A. Lapa dos Morcegos (LM) B. Pau d'alho (PD) C. Crevice Cave (CC) B_z (nT) 1 cm

Figure 4. Overlay of superconducting quantum interference device (SQUID) microscopy maps on images for the three stalagmites analyzed here. Out-of-the-page magnetic field component (B_z) maps were measured ~200 µm above the samples. Color scale on the right is the same for all three samples. We notice strong correlation between the strength of the remanent magnetic field and the darkness of speleothem bands for samples from (a) Lapa dos Morcegos Cave (LM) and (b) Pau d'Alho Cave (PD), indicating layers that are rich in magnetic minerals. We do not observe such pattern in the thick section from (c) Crevice Cave (CC), suggesting a lower concentration of magnetic minerals in this sample.

obtained at an effective sensor-to-sample distance of $\sim 300 \, \mu m$ inside a magnetically shielded room. We retrieved magnetic moments from the SQUID microscopy maps by using the inversion technique described in Lima et al. (2023). PD and CC samples were mapped parallel to their growth direction and the corresponding magnetic moments were rotated to match the direction of the growth axis, while LM samples were mapped perpendicular to the growth axis (Figure 1). The directions of NRM components were calculated using principal component analysis (PCA) (Kirschvink, 1980). If a NRM component had a deviation angle less than the maximum angular deviation (MAD), then this component was inferred to be the characteristic component and therefore anchored to the origin (Kirschvink, 1980; Tauxe & Staudigel, 2004).

Following the completion of the AF demagnetization sequence, we applied a series of repeated anhysteretic remanent magnetization (ARM) steps to each sample to establish the robustness of the magnetic records retrieved. The accuracy and precision of these ARM applications are useful for determining whether the concentration of magnetic minerals in each individual sample is sufficiently high to acquire a magnetization in the direction of an applied field. We use the ARM as a proxy for the DRM and/or CRM of the speleothems, an assumption that supported by paleointensity studies with speleothems (Ponte et al., 2018). We conducted five independent ARM applications for each sample. To quantitatively determine how well a sample can acquire magnetization direction, we calculated the ΔARM parameter (Figure 2), defined as:

$$\Delta ARM = \frac{1}{2} \sqrt{\frac{1}{N} \sum_{i=1}^{N} \left[\sin(inc_{lab}) - \sin(inc_{sample,i}) \right]^2},$$
 (1)

where N is the number of ARM applications, inc_{lab} is the expected inclination of the application of the ARM along the z-axis (i.e., $inc_{lab} = 90^{\circ}$ or $inc_{lab} = -90^{\circ}$), and $inc_{sample,i}$ is the measured magnetic inclination of the sample's remanence after ARM application i out of N. The 0.5 factor in front of the expression normalizes the parameter between 0 and 1. The ΔARM parameter accounts for both systematic deviations (e.g., magnetic anisotropy) and random deviations (e.g., scatter in the magnetization acquisition) from the expected direction and provides an estimation of how well a sample can acquire magnetic direction. For $inc_{lab} = -90^{\circ}$, a value of $\Delta ARM = 0$ indicates that all ARM acquisitions are in the same direction as the ARM application, while an $\Delta ARM = 1$ indicates that all the ARM acquisitions are in the opposite direction from the ARM application. For reference, five

BORLINA ET AL. 6 of 20

.wiley.com/doi/10.1029/2024GC011594 by University Of

ota Lib, Wiley Online Library on [13/11/2024]. See the Terms

Table 1
Summary of Components From Alternating Field Demagnetization From LM Samples

Sample	Component	Range (mT)	Declination (°)	Inclination (°)	MAD (°)	DANG (°)	Anchored?
LM.1	LC	0–5	34.5	-51.8	-	-	-
	HC	5–25	301.3	62.5	5.1	3.3	Y
LM.2	HC	0-32	308.3	52.1	7.8	17.9	Y
LM.3	LC	0–5	335.7	-6.3	-	_	_
	HC	5-40	322.7	55.2	7.6	16.9	N
LM.4	LC	0-40	314.4	53.9	8.6	8.0	Y

Note. The first column lists the sample name, the second column lists the name of the component (LC for low coercivity and HC for high coercivity), the third column lists the range used to calculate the fit in mT, the fourth, fifth and sixth columns show the results of the principal component analysis, which include the declination, inclination and maximum angular deviation (MAD), the seventh column lists the deviation angle (DANG) for the component, and the eighth column denotes whether the component is anchored (Y for yes and N for no).

measured ARM applications that are either systematically 25° off the correct ARM direction or have a 25° scatter around the correct direction will have $\Delta ARM \sim 0.047$. Ultimately, the choice of the bias field used to calculate the ΔARM will depend on the expected strength of the intensity of the paleomagnetic field. For instance, some of the

 Table 2

 Summary of Components From Alternating Field Demagnetization From S1 Samples

Sample	Component	Range (mT)	Declination (°)	Inclination (°)	MAD (°)	DANG (°)	Anchored?
S1.1	LC	0–5	104.1	-29.1	16.8	-	-
	HC	5-22.5	324.2	6.7	5.8	3	Y
S1.2	LC	0-2.5	97.1	56.7	-	-	-
	HC	5-22.5	85.5	60.4	14.8	7.4	Y
S1.3	LC	0-2.5	80	10.9	-	-	-
	HC	2.5–35	99.6	-20.9	39	98.2	N
S1.4	LC	0-15	223.2	40.5	29.3	-	-
	HC	15-47.5	108.7	-3.3	44.4	71.5	N
S1.5	LC	0–5	166.4	-49.4	9.4	_	-
	HC	5-30	345.1	68.2	21.8	28.1	N
S1.6	LC	0-2.5	65.9	3.9	0	-	-
	HC	2.5–30	20.7	20.3	18.7	28.9	N
S1.7	LC	0-7.5	282.2	-41.7	17.6	-	-
	HC	7.5–27.5	40.1	-4.4	13	15.3	N
S1.8	LC	0–5	301.3	38.7	15.2		-
	HC	5–20	19.5	-18.9	25.9	23.9	Y
S1.9	HC?	0-30	249.8	12.8	28.1	115.7	N
S1.10	LC	0-25	350.6	-34	35.3	-	-
	HC	25-45	154.6	12.1	22.6	24.7	N
S1.11	HC	0-30	28.2	-39.7	44.3	55.9	N
S1.12	LC	0-7.5	189.5	18.1	28.3	_	-
	НС	7.5–17.5	346	33.7	8.9	41.4	N

Note. The first column lists the sample name, the second column lists the name of the component (LC for low coercivity and HC for high coercivity), the third column lists the range used to calculate the fit in mT, the fourth, fifth and sixth columns show the results of the principal component analysis, which include the declination, inclination and maximum angular deviation (MAD), the seventh column lists the deviation angle (DANG) for the component, and the eighth column denotes whether the component is anchored (Y for yes and N for no).

BORLINA ET AL. 7 of 20

Table 3Summary of Components From Alternating Field Demagnetization From S3 Samples

Sample	Component	Range (mT)	Declination (°)	Inclination (°)	MAD (°)	DANG (°)	Anchored
S3.1	HC?	0-50	130.8	-30.7	45.7	161.2	N
S3.2	LC	0–5	97.2	-42.2	-	_	-
	HC	10-25	43.3	9.1	35.5	39.9	-
S3.3	LC	0–10	30.9	19.3	20	-	-
	HC	20-30	347.1	-22.1	34.3	38.7	N
S3.4	LC	0–5	88.1	41.8	0	-	-
	HC	5-50	18.5	-1.1	9.4	8.4	Y
S3.5	LC	0–10	180.8	42	9.6	-	-
	HC	10-50	6	-2.4	7.5	3.6	Y
S3.6	LC	0-10	341.6	27.7	4.3	-	-
	HC	10–45	14.5	-20	28.1	32.9	N

Note. The first column lists the sample name, the second column lists the name of the component (LC for low coercivity and HC for high coercivity), the third column lists the range used to calculate the fit in mT, the fourth, fifth and sixth columns show the results of the principal component analysis, which include the declination, inclination and maximum angular deviation (MAD), the seventh column lists the deviation angle (DANG) for the component, and the eighth column denotes whether the component is anchored (Y for yes and N for no).

studied speleothems contain records of the South Atlantic Anomaly and of magnetic excursions, and we chose to use a 30 μ T bias field to more accurately assess the recording capabilities of the speleothems during such events. For times when the geomagnetic field is stronger, this lower bias field places an upper limit on the directional error of these samples.

3. Results

The FORC diagrams of the two PD samples from S3 show similar features, but with S3.5 having a signal strength more than twice that of S3.1 (Figures 3a and 3b). Both FORC diagrams have a low-coercivity central ridge along the horizontal axis characteristic of non-interacting single domain (SD) particles ($<0.1~\mu m$) (Harrison & Lascu, 2014). The central ridge coercivity distribution spans the interval 0–65 mT, with a peak amplitude near the origin. The background signal, with increasing spread closer to the vertical axis, is typical of $<0.1-5~\mu m$ -sized particles in the pseudo-single domain state characterized by single vortex and multivortex configurations (Lascu et al., 2018; Roberts et al., 2017). Similar results are observed in the FORC diagrams from the samples obtained from LM1 (Figures 3c and 3d). The FORCs from the LM1 samples show the central ridge like those from the S3

Table 4Summary of Components From Alternating Field Demagnetization From S5 Samples

Sample	Component	Range (mT)	Declination (°)	Inclination (°)	MAD (°)	DANG (°)	Anchored?
S5.1	NA	0-50	224.6	60.4	20	-	-
S5.2	LC	0-10	247.1	-65.8	12	-	-
	HC	10-50	65	56.2	11.9	21.8	N
S5.3	LC	0–5	102.1	-3.4	_	_	_
	HC	10-35	48.7	-34.3	18	69.5	N
S5.4	LC	0–5	156.9	-37.6	_	_	_
	HC	5–30	114.7	-52.9	33	80.4	N

Note. The first column lists the sample name, the second column lists the name of the component (LC for low coercivity and HC for high coercivity), the third column lists the range used to calculate the fit in mT, the fourth, fifth and sixth columns show the results of the principal component analysis, which include the declination, inclination and maximum angular deviation (MAD), the seventh column lists the deviation angle (DANG) for the component, and the eighth column denotes whether the component is anchored (Y for yes and N for no).

BORLINA ET AL. 8 of 20

are governed by the applicable Creati

Sample	Component	Range (mT)	Declination (°)	Inclination (°)	MAD (°)	DANG (°)	Anchored?
CC.1	_	0–50	326.1	17.1	35.1	76.2	_
CC.2	-	0-50	32.2	-39.1	30.8	113.7	-
CC.3	-	0-50	273.6	27	30.4	73.3	-
CC.4	-	0-50	17.2	-12.9	14.9	160.2	-

Note. The first column lists the sample name, the second column lists the name of the component (LC for low coercivity and HC for high coercivity), the third column lists the range used to calculate the fit in mT, the fourth, fifth and sixth columns show the results of the principal component analysis, which include the declination, inclination and maximum angular deviation (MAD), the seventh column lists the deviation angle (DANG) for the component, and the eighth column denotes whether the component is anchored (Y for yes and N for no).

samples, indicative of SD particles. The central ridge spans coercivities of 0–65 mT, similar to that of the S3 samples. The background signal is also similar to that of the S3 samples, indicating the presence of a vortex component. Because the masses of the LM samples were not measured, it is not possible to directly compare the intensity per unit mass between samples from PD and LM. The central ridge of LM1.52 appears narrower than that of the other samples because of the higher measurement resolution of this sample.

NRM field maps of the thick sections of each speleothem prior to cutting the longitudinal strips are shown in Figure 4. We observe that the PD thick section has the strongest magnetic field sources from all the sections, demonstrating clear correlation between dark bands and strong magnetic field signal. We also observe strong and weak magnetic signals alternating across the PD sample. A strong magnetic field signal is also observed on the edges of the PD thick section, where stalagmite layers merge. Compared to the PD sample, a less pronounced banding pattern in the magnetic signal is observed within the thick section of the LM stalagmite. In the LM thick

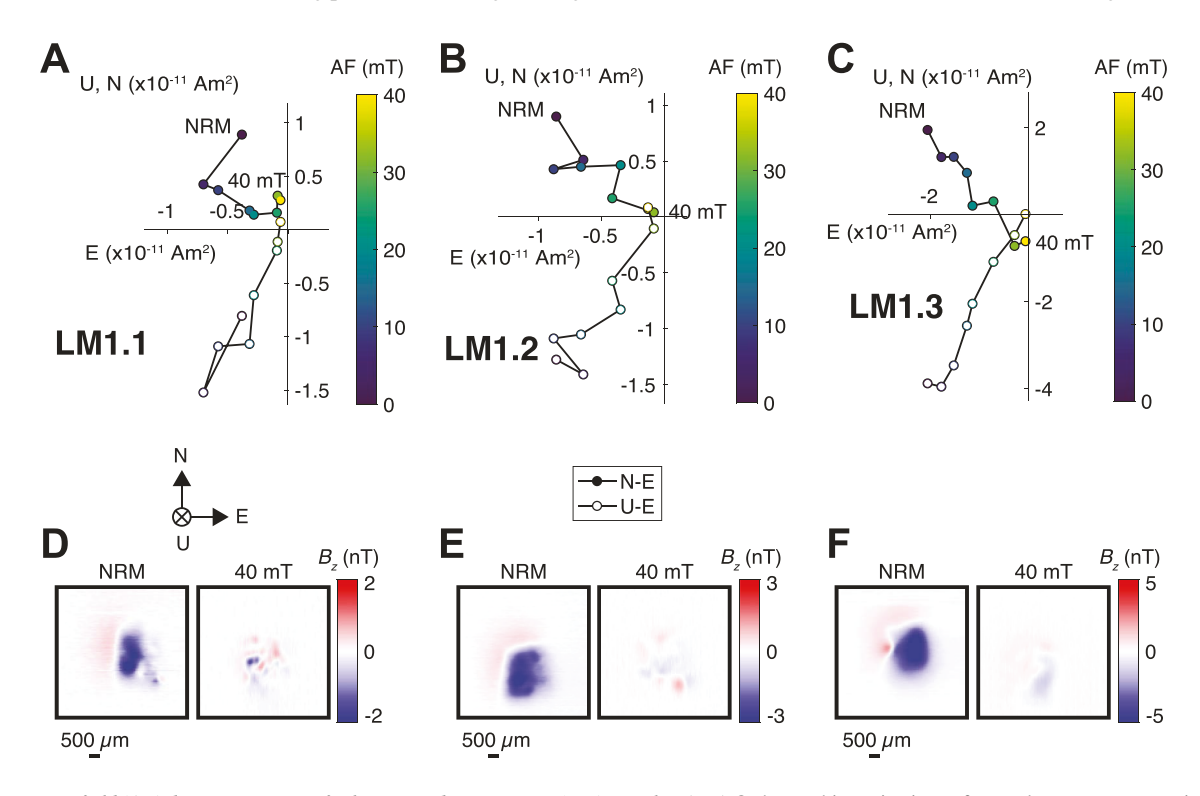


Figure 5. Alternating field (AF) demagnetization of select Lapa dos Morcegos (LM) samples. (a–c) Orthographic projections of natural remanent magnetization (NRM) vector endpoints during AF demagnetization. Closed symbols represent the north-east (N-E) projection of the magnetic moment and open symbols represent the up-east (U-E) projection of the magnetic moment. Color scales show the AF level. (d–f) Out-of-the-page magnetic field component (B_z) maps for select steps measured at a height of ~300 μ m above the samples obtained with the superconducting quantum interference device (SQUID) microscope. Coordinate system refers to measurements coordinates for the SQUID microscope maps.

BORLINA ET AL. 9 of 20

15252027, 2024, 10, Downloaded from https://agupubs.onlinelibrary.wiley.com/doi/10.1029/2024GC011594 by University Of Minnesota Lib, Wiley Online Library on [13/11/2024]. See the Terms

and Conditions

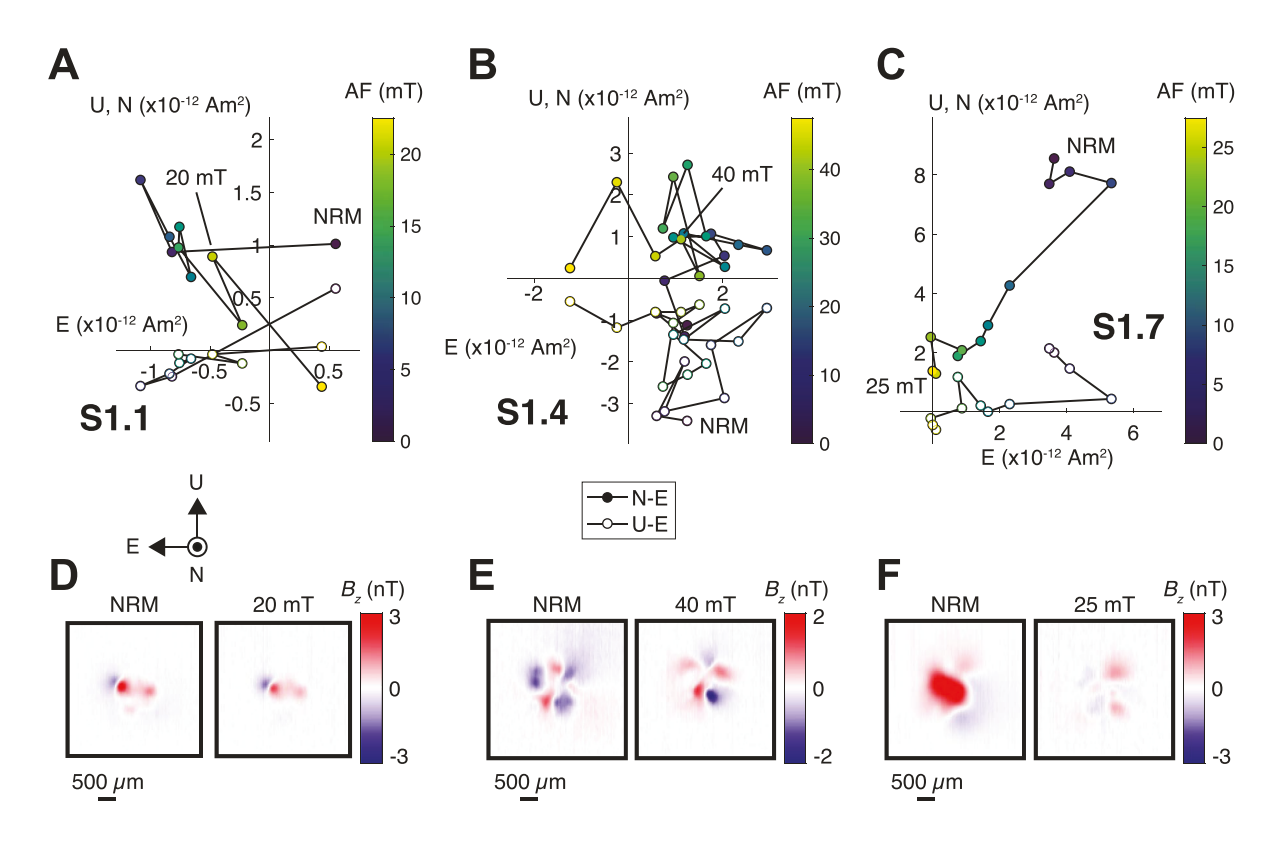


Figure 6. Alternating field (AF) demagnetization of select Pau d'Alho (PD) STRIP1 samples. (a–c) Orthographic projections of natural remanent magnetization (NRM) vector endpoints during AF demagnetization. Closed symbols show the north-east (N-E) projection of the magnetic moment and open symbols represent the up-east (U-E) projection of the magnetic moment. Color scales show the AF levels. (d–f) Out-of-the-page magnetic field component (B_z) maps for selected steps measured at a height of ~300 µm above samples obtained with the superconducting quantum interference device (SQUID) microscope. Coordinate system refers to measurements coordinates for the SQUID microscope maps.

section, we observe alternating layers of positive and negative fields, suggesting either rapid variations in the magnetic field recorded in the samples or weak regions of magnetic field signal that allow for fringing fields from strong magnetic bands to appear. The CC thick section shows the strongest signals on the edges of the sample, and we do not observe the clear banding associated with magnetic field signal across layers as identified in the other two speleothems. Overall, the magnetic signal of the CC samples is noticeably weaker than that of the other two speleothems.

AF demagnetization of the speleothem samples generally revealed two NRM components, usually with a low coercivity component between 5 and 10 mT and a high coercivity (HC) component between 20 and 50 mT. We summarize the PCA components of all samples in Tables 1–5. We also present select plots of the orthographic projections of NRM vector endpoints in Figures 5–9. Additionally, Figures 10–12 summarize the inclination, declination, MAD and ΔARM for our samples. All demagnetized samples from the LM stalagmite had components (Figures 5 and 10). PD samples showed more variability across sizes and samples, resulting in demagnetizations that ranged from noisy to origin-trending components (Figures 6–8, and 11). Finally, CC samples did not produce any discernible components during demagnetization (Figures 9 and 12).

We also report on the comparison between data sets obtained with traditional paleomagnetic techniques and those obtained here using the SQUID microscope. Figures 13 and 14 show this comparison for the measurements obtained from the LM and PD samples. We do not report the same comparison for the CC samples because of their lack of stable magnetic components observed in the SQUID microscopy measurement sequences.

BORLINA ET AL. 10 of 20

15252027, 2024, 10, Downloaded from https://agupubs.onlinelibrary.wiley.com/doi/10.1029/2024GC011594 by University Of Minnesota Lib, Wiley Online Library on [13/11/2024]. See the Terms and Conditions (https://agupubs.onlinelibrary.wiley.com/doi/10.1029/2024GC011594 by University Of Minnesota Lib, Wiley Online Library on [13/11/2024]. See the Terms and Conditions (https://agupubs.onlinelibrary.wiley.com/doi/10.1029/2024GC011594 by University Of Minnesota Lib, Wiley Online Library on [13/11/2024]. See the Terms and Conditions (https://agupubs.onlinelibrary.wiley.com/doi/10.1029/2024GC011594 by University Of Minnesota Lib, Wiley Online Library on [13/11/2024]. See the Terms and Conditions (https://agupubs.onlinelibrary.wiley.com/doi/10.1029/2024GC011594 by University Of Minnesota Lib, Wiley Online Library on [13/11/2024]. See the Terms and Conditions (https://agupubs.onlinelibrary.wiley.com/doi/10.1029/2024GC011594 by University Of Minnesota Lib, Wiley Online Library.wiley.com/doi/10.1029/2024GC011594 by University Of Minnesota Library.wiley.com/doi/10.

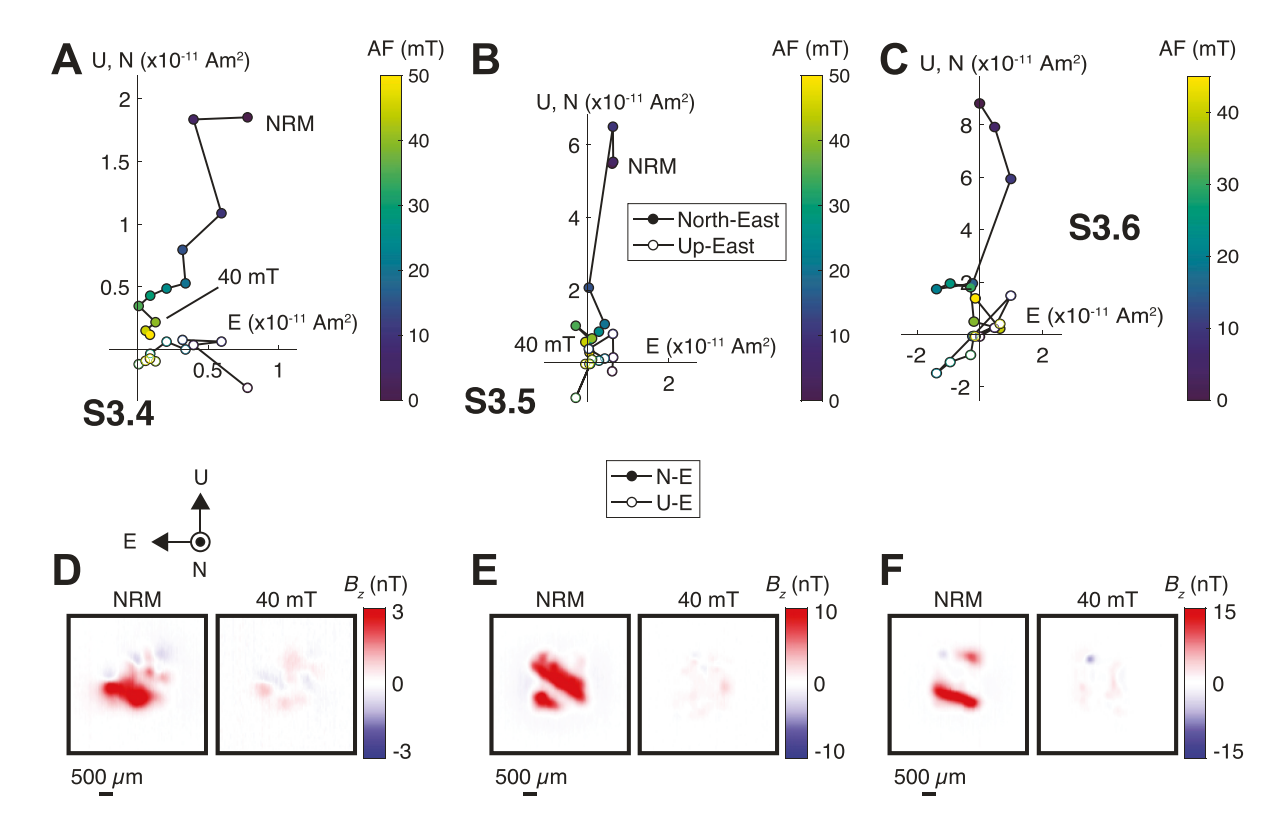


Figure 7. Alternating field (AF) Demagnetization of selected Pau d'Alho (PD) STRIP3 samples. (a–c) Orthographic projections of natural remanent magnetization (NRM) vector endpoints during AF demagnetization. Closed symbols show the north-east (N-E) projection of the magnetic moment and open symbols represent the upeast (U-E) projection of the magnetic moment. Color scales show the AF levels. (d–f) Out-of-the-page magnetic field component (B_z) maps for selected steps measured at a height of ~300 μ m above samples obtained with the superconducting quantum interference device (SQUID) microscope. Coordinate system refers to measurements coordinates for the SQUID microscope maps.

4. Discussion

4.1. Obtaining Magnetic Moments From Speleothem Samples

A distinctive aspect of this study is that, compared to previous studies of isolated zircon grains and chondrules (e.g., Borlina et al., 2020, 2021; Fu, Lima, & Weiss, 2014; Fu, Weiss, et al., 2014; Fu et al., 2017), speleothem samples exhibit predominantly non-dipolar fields in SQUID microscopy maps (Figures 5d–5f, 6d–6f, 7d–7f, 8d–8f, and 9d–9f). The non-dipolarity of the speleothem samples is likely associated with the nature of the magnetic acquisition process, the size of the samples and the fact that many of the magnetic sources are polymineralic assemblages of clays, oxides and organic matter. Overall, retrieving the net magnetic moment from speleothem samples using magnetic microscopy requires using multipolar inversion techniques (compare Lima et al. (2023) with Lima and Weiss (2016)).

4.2. Variability of Magnetic Properties Between Different Speleothems

From these speleothems we observed three different behaviors. First, the LM stalagmite section showed NRM homogeneity across samples, consistent with the overall homogeneous magnetic intensity of the NRM of the thick section (Figure 4a) and the measured low ΔARM values (Figure 10d). We also observed well-constrained HC components during AF demagnetization (Figure 5), and excellent agreement between the data measured in larger volumes and those obtained with SQUID microscopy (13). Overall, these observations indicate that this stalagmite is an excellent target for future paleomagnetic studies with the goal of obtaining high-resolution temporal magnetic records. In fact, this sample can provide an improvement of at least 5 times in the temporal resolution of the magnetic record compared to that obtained with traditional paleomagnetic instrumentation.

BORLINA ET AL. 11 of 20

15252027, 2024, 10, Downloaded from https://agupubs.onlinelibrary.wiley.com/doi/10.1029/2024GC011594 by University Of Minnesota Lib, Wiley Online Library on [13/11/2024]. See the Terms and Conditions

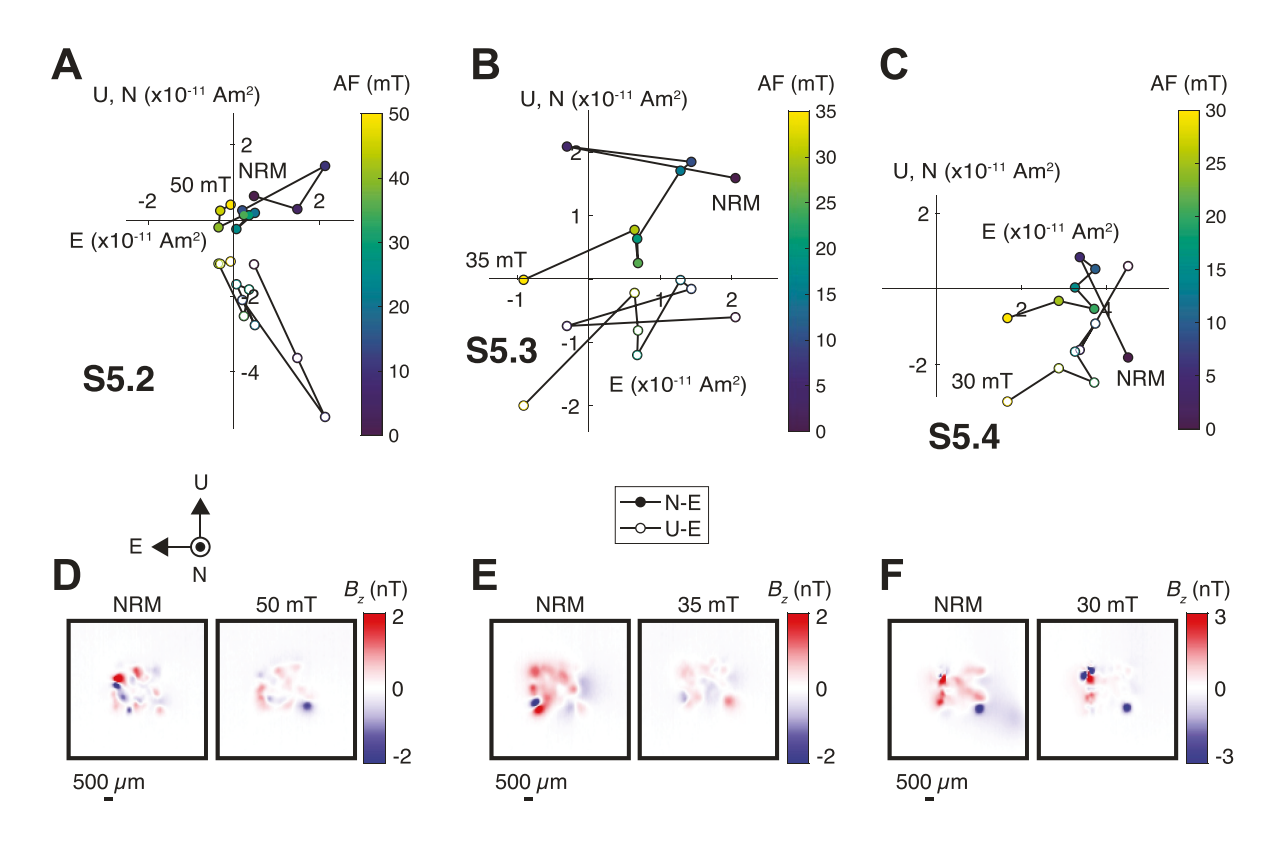


Figure 8. Alternating field (AF) demagnetization of select Pau d'Alho (PD) STRIP5 samples. (a–c) Orthographic projections of natural remanent magnetization (NRM) vector endpoints during AF demagnetization. Closed symbols show the north-east (N-E) projection of the magnetic moment and open symbols represent the up-east (U-E) projection of the magnetic moment. Color scales show the AF levels. (d–f) Out-of-the-page magnetic field component (B_z) maps for selected steps measured at a height of ~300 µm above samples obtained with the superconducting quantum interference device (SQUID) microscope. Coordinate system indicates the original direction of the measurements obtained with the SQUID microscope compared to the ones reported in the orthographic projections.

The second type is represented by the PD stalagmite, which showed variable magnetic properties along the growth axis. We observed large variations in the strength of the NRM field of the thick section that correlates with the banding seen in the image of the sample (Figure 4b) and the variations in the ΔARM parameter (Figures 11j–11l). These variations are further highlighted by the observation that some samples present HC components (e.g., Figures 6c, 7a, and 8a) while other samples do not show well-constrained components (e.g., Figures 6b and 8b). Similar variations are observed by comparing the results from this study to that of Trindade et al. (2018). The direction and its associated MAD from some samples include the data from Trindade et al. (2018) while others do not (Figure 14). In summary, the PD stalagmite has varying concentrations of magnetic minerals across the growth axis and if a uniform sampling size is employed for SQUID microscopy studies, some regions will produce reliable magnetic records while others might not. Nonetheless, the regions with strongest NRM signal indicating high concentration of magnetic minerals in this speleothem can help improve the current magnetic record by a factor of 2–3 times. Below, we discuss the effect of different sample sizes in the paleomagnetic results and how sample size can help produce more consistent and robust results in heterogeneous speleothems.

The third type is represented by the CC sample. This speleothem has a lower concentration of magnetic minerals as demonstrated by the very weak magnetic fields observed in the SQUID microscope NRM map (Figure 4c) and by the consistently high ΔARM values (Figure 12d). The lack of discernible NRM components (Figure 9) further indicates that this sample has poor recording properties at the small spatial scales associated with micropaleomagnetic studies. Owing to the lower concentration of magnetic minerals, intrinsic to this speleothem, we observe that these samples do not have enough magnetic carriers to be analyzed in such small volumes, compared to that used by Lascu et al. (2016). Such speleothems can be more successfully studied using traditional bulk sample methods, but are not amenable to temporal resolution improvements from micro-paleomagnetic studies.

BORLINA ET AL. 12 of 20

15252027, 2024, 10, Downloaded from https://agupubs.onlinelibrary.wiley.com/doi/10.1029/2024GC011594 by University Of Minnesota Lib, Wiley Online Library on [13/11/2024]. See the Terms and Conditions

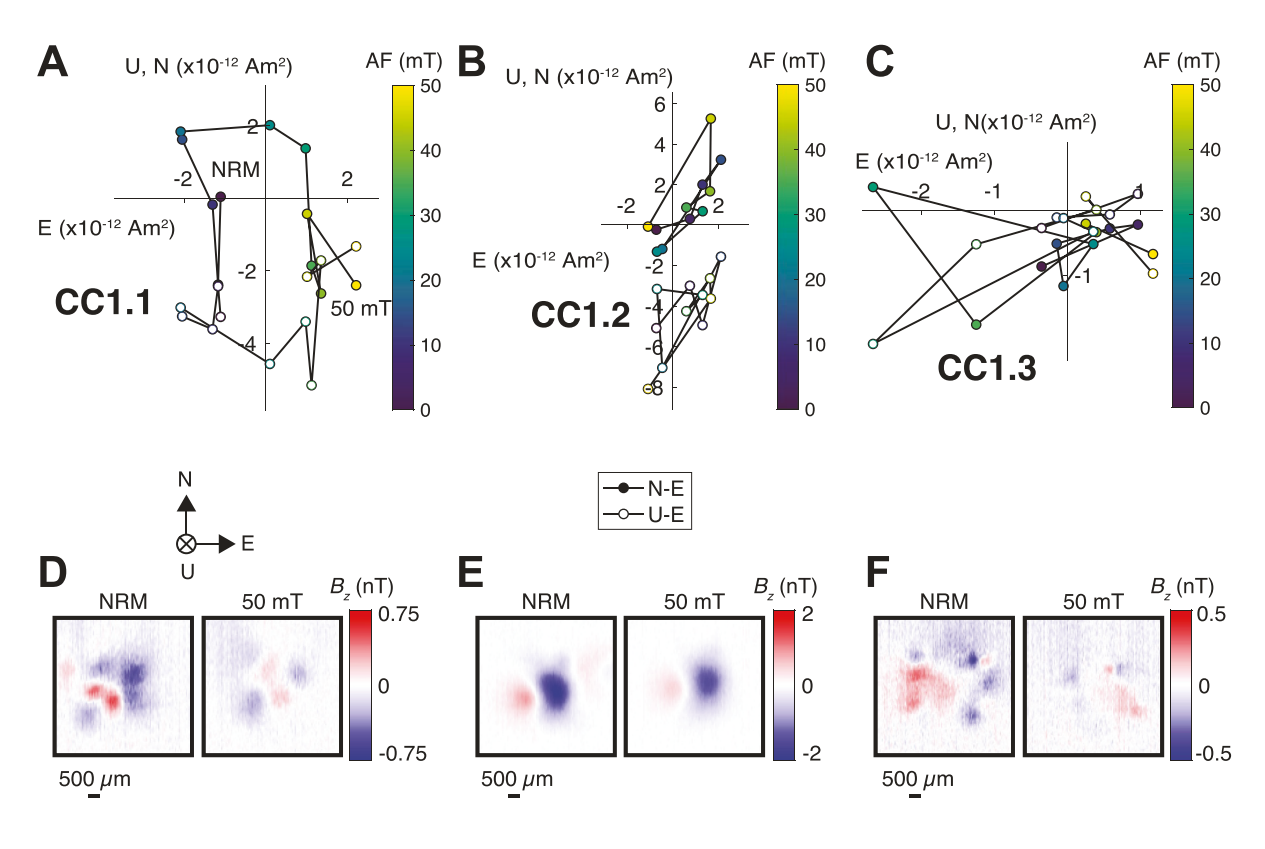


Figure 9. Alternating field (AF) demagnetization of select Crevice Cave (CC) samples. (a–c) Orthographic projections of natural remanent magnetization (NRM) vector endpoints during AF demagnetization. Closed symbols show the North-East projection of the magnetic moment and open symbols show Up-East projection of the magnetic moment. Color scales show the AF levels. (d–f) Out-of-the-page magnetic field component (B_z) maps for selected steps measured at a height of ~300 µm above samples obtained with the superconducting quantum interference device (SQUID) microscope. Coordinate system indicates the original direction of the measurements obtained with the SQUID microscope compared to the ones reported in the orthographic projections.

In summary, the three speleothems analyzed represent different examples in a range of magnetic properties of speleothems: (a) speleothems with magnetic properties similar to those of the CC speleothem do not benefit from high-resolution analysis, as the temporal resolution of their magnetic record cannot be meaningfully improved beyond that obtained with traditional paleomagnetic instrumentation; (b) speleothems like LM allow for an improvement in temporal resolution of the magnetic record by a factor of five or better; (c) speleothems like PD represent an intermediate example between those two endmembers, with regions of low concentration of magnetic carriers that may not benefit from high-resolution analysis, and others that allow for a meaningful temporal resolution improvement. Ultimately, we are limited by the characteristics of a given speleothem and not by the instrumental technique when obtaining high-temporal-resolution paleomagnetic records from speleothems: there must be enough magnetic carriers in a small-volume sample capable of statistically recording the magnetic field.

4.3. Variability of Magnetic Properties in Speleothems

4.3.1. Magnetic Mineralogy of a Heterogeneous Speleothem

Both PD and LM show variations in the amount of magnetic carriers across their growth axis with the variations being more pronounced in the PD sample (Figure 4). Magnetic variability in a speleothem can emerge from at least three scenarios: (a) the NRM is weak because Earth's magnetic field was weak during magnetic acquisition, (b) the concentration of magnetic minerals changes across the speleothem or (c) the composition of magnetic minerals changes across the speleothem. For the first case, the ΔARM parameter can help determine if the weak magnetization from a speleothem comes from the actual magnetic field of the Earth or from the magnetic properties of the sample. As discussed above, this is unlikely to be the case for the samples observed here. We now focus on the other two cases. The FORC analysis shown in Figure 3 from two PD samples (S3.1 and S3.5) helps differentiate between these two cases. The FORC diagram supports the presence of fine-grained magnetite and

BORLINA ET AL. 13 of 20

onlinelibrary.wiley.com/doi/10.1029/2024GC011594 by University Of Minnesota Lib, Wiley Online Library on [13/11/2024]. See the Terms

LM ~4 mm³

o uoita uijui -40

-80

14800 14900 15000 15100
Age (years CE)

180

180

14800 14900 15000 15100

Age (years CE)

Age (years CE)

50
40
30
10
14800 14900 15000 15100

Age (years CE)

0.2

0.15

0.15

0.05

14800 14900 15000 15100

Age (years CE)

6, 3 'S, 2 8:S 'S: 8: 8: 8: 8: 7

> & ?8; 5:?& E ')

> > , :: :

3

 ?8; 5:?&
 '
 '
 '
)
 69 (

 ?2; ?
 %
 %
 '
 '
 '
 '
 '
 '
 '
 '
 '
 '
 '
 '
 '
 '
 '
 '
 '
 '
 '
 '
 '
 '
 '
 '
 '
 '
 '
 '
 '
 '
 '
 '
 '
 '
 '
 '
 '
 '
 '
 '
 '
 '
 '
 '
 '
 '
 '
 '
 '
 '
 '
 '
 '
 '
 '
 '
 '
 '
 '
 '
 '
 '
 '
 '
 '
 '
 '
 '
 '
 '
 '
 '
 '
 '
 '
 '
 '
 '
 '
 '
 '
 '
 '
 '
 '
 '
 '
 '
 '
 '
 '
 '
 '
 '
 '
 '
 '
 '
 '
 '
 '
 '
 '
 '
 '
 '
 '
 '

8 ? ; -:?

S

, :: : 0 & ' 8 & % & ,:) ' ' 3 86 ' 4 5: ' ' (@) ?& ')) ' (@)

& & % & % & ...
)) & ?8;5:86' :
) & & ...

& % S

E ...
3 '8 4 % 3 & ...

&

:?

) E '

?&

15252027, 2024, 10, Downloaded from https://agupubs.onlinelibrary.wiley.com/doi/10.1029/2024GC011594 by University Of Minnesota Lib, Wiley Online Library on [13/11/2024]. See the Terms and Conditions

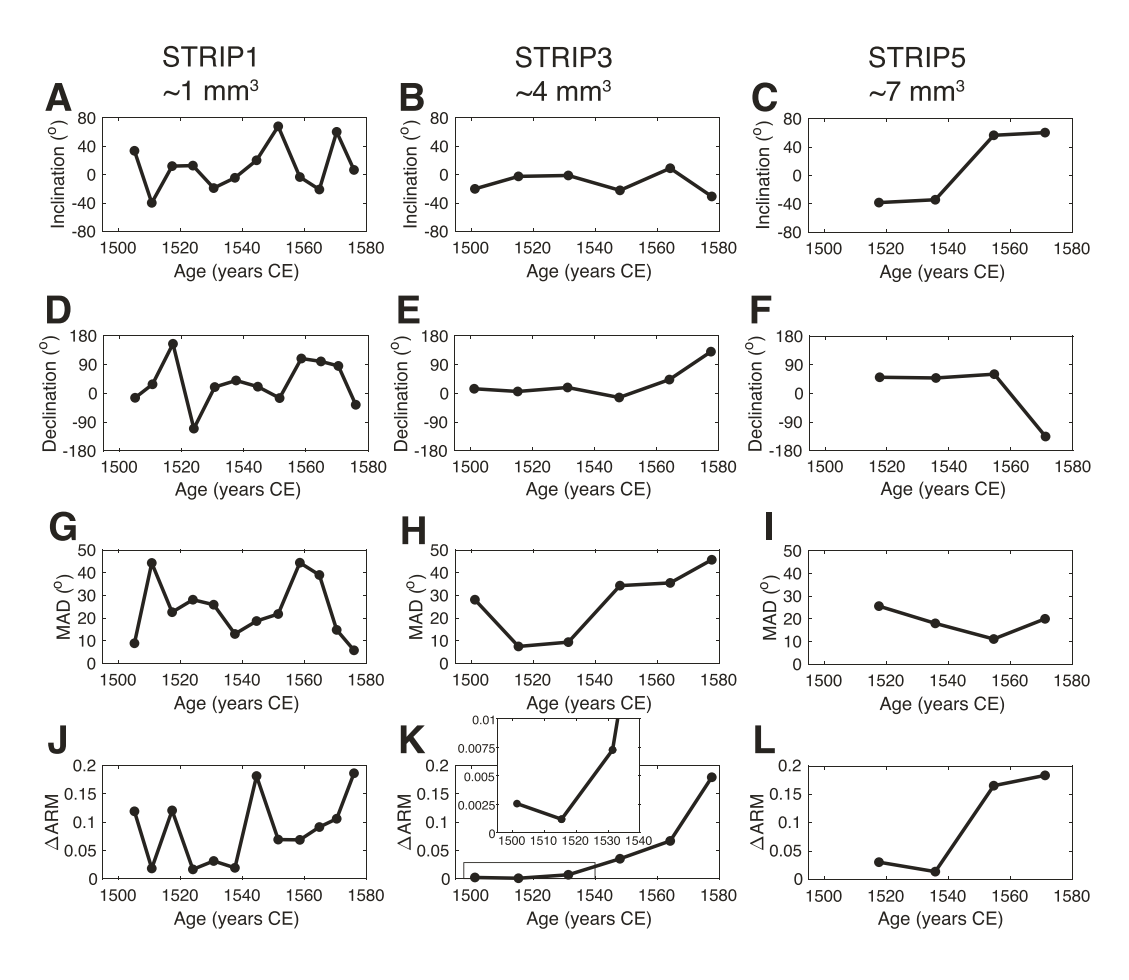


Figure 11. Summary of magnetic directions, maximum angular deviation (MAD) and \triangle ARM values as a function of age for the Pau d'Alho (PD) (STRIP1, STRIP3 and STRIP5) samples. Shown are plots for (a) inclination, (d–f) declination, (g–i) MAD and (j–l) \triangle ARM. An inset in panel (k) is presented to show the smallest \triangle ARM values.

of ALHO06 from which we obtained our samples did not originate from an area with horizontal growth layers, but from an area with dipping layers off-center from the central growth axis (Figure 1b). Previous studies have suggested that magnetic records from samples obtained from regions with dipping growth surfaces are not significantly distinct from those that are not horizontal (e.g., Latham et al., 1989; Lean et al., 1995; Morinaga et al., 1989; Openshaw et al., 1997). Nonetheless, a recent study has suggested that this effect might be significant (Ponte et al., 2017). In the case of the stalagmite studied by Ponte et al. (2017), magnetic inclinations increase up to 5° depending on the position of the sample along the flank of the stalagmite. While there is no consistent systematic offset between our data sets and that of the previous study (Figure 14), future work needs to focus on how the slope across a speleothem might affect the magnetic record at finer spatial scales, and micropaleomagnetism can be used to investigate those questions.

4.4. Dating Speleothems for Micro-Paleomagnetic Studies

Speleothems with higher concentrations of magnetic minerals generally produce better magnetic results. In some cases, this may pose a challenge to the U-Th system used for dating speleothems, as the presence of allochthonous mineral phases that produce the magnetic signal also contaminates the sample with detrital thorium (Lascu & Feinberg, 2011). This suggests that speleothems that are ideal paleomagnetic recorders might not necessarily yield the highest accuracy U-Th dates. The degree to which the allochthonous phases hamper the U/Th dating technique varies on an individual sample basis and reflects a number of variables including the uranium concentration, the ²³²Th concentration, the degree to which the ²³⁰Th/²³²Th value of the detrital component can be constrained through the application of isochrons, and the sample age. This is best assessed on a case-by-case

BORLINA ET AL. 15 of 20

CC ~1.2 mm³ Inclination (°) 40 0 -40 -80 24000 25000 26000 27000 Age (years B.P.)

24000 25000 26000 27000 Age (years B.P.)

C 50 (°) 30 30 20 10 25000 26000 24000 27000 Age (years B.P.)

D 0.4 0.3 ₩₩ 0.3 0.2 0.1 0 26000 24000 25000 27000 Age (years B.P.)

3 8): 8: 8: 8 : S

)

?) Е E 8??& C 3 Η :?9 C Н

' ?9 **@** ; -N& ? ; 5:?

 \mathbf{C} 3 @3) 3 8& W 8 ? ; -N O ; -:?9 C & ?((

8??6') ?& ?8; -:) Е Е

?& C V 6 @ E 86 ' % @ ?

8??(?; 5N C ? ? ; 5: @ N ? 8?? ? :? S

; R

onlinelibrary.wiley.com/doi/10.1029/2024GC011594 by University Of Minnesota Lib, Wiley Online Library on [13/11/2024]. See the Terms and Conditions (http

Н

Н

15252027, 2024, 10, Downloaded from https://agupubs

onlinelibrary.wiley.com/doi/10.1029/2024GC011594 by University Of Minnesota Lib, Wiley Online Library on [13/11/2024]. See the Term

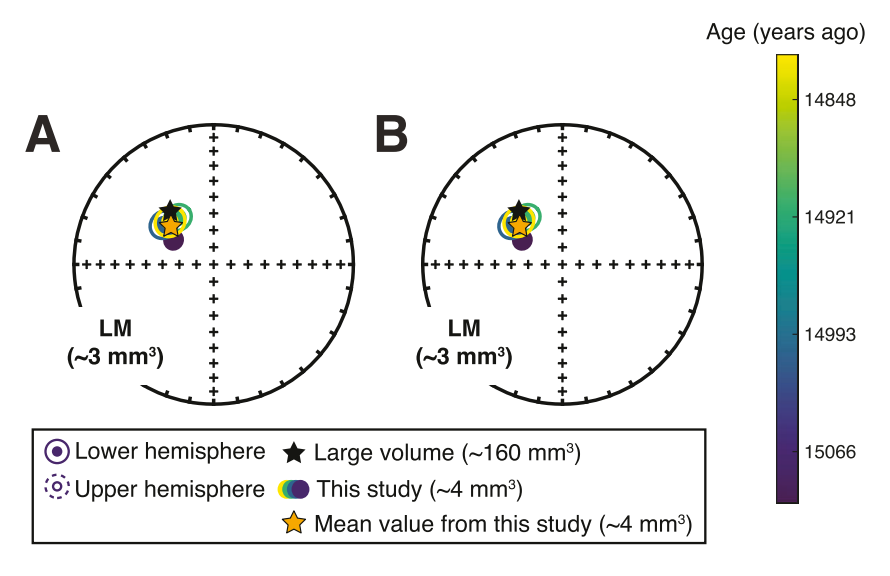


Figure 13. Comparison between high coercivity directions measured with traditional paleomagnetic techniques and by superconducting quantum interference device (SQUID) microscope for Lapa dos Morcegos (LM) samples. (a) Equal area stereographic projections showing all directions obtained from LM1. (b) Equal area stereographic projections showing directions with samples that presented $\Delta ARM < 0.047$ from the same samples as (a). No samples were excluded by this selection criterion in this case. Black star is the measurement for this sample using traditional paleomagnetic techniques (\sim 1,600 mm³), circles are the SQUID microscope results from this study with color scales indicating the ages of the samples, and yellow star is the average direction of the results from this study.

example, can help provide information about the robustness of the direction obtained from the magnetic record of a sample based on its magnetic properties.

4.6. Workflow for Future Work on Speleothem Micro/Paleomagnetism

We demonstrate that robust records can be obtained from small-volume samples using SQUID microscopy, and we devised the following additional protocols for future studies of micro-paleomagnetism with speleothems to improve accuracy and optimize temporal resolution. First, in the methodology section, we described using nonrecycled water during the cutting process of some samples. This is important since sample preparation is key to generally avoid contamination and re-deposition of speleothem particles with random orientations onto the porous surface of the sample that later could negatively impact sample measurements. Given the very small volume of these samples, contamination may easily affect a non-negligible fraction of the moment and result in a larger scatter during NRM demagnetization. Second, repeat AF applications and measurements are beneficial to reduce the uncertainty in the estimation of the magnetic components. Here, we performed a single measurement for a single AF step. For future studies, we recommend using three to five repeat AF applications and moment measurements per AF level to decrease the scatter associated with the AF demagnetization process in speleothems and the low signal-to-noise ratio in some maps. Finally, because some samples might be magnetically heterogeneous (e.g., PD sample), it is important to start with a NRM map and a test strip to determine which regions of the speleothem can be sampled finer and targeted in higher resolution. An initial SQUID microscope map of a speleothem thick section, such as the ones shown in Figure 4, can be used to discern the regions with higher magnetic signals from which smaller volumes can be extracted. This will help determine which regions have a higher (lower) concentration of magnetic carriers producing finer (coarser) magnetic records across the speleothem. Additionally, initial analysis using the SQUID microscope of samples adjacent to the main section of the targeted speleothem can help determine how the speleothem should be subsampled such that the targeted material is adjusted to yield similar small values for $\triangle ARM$. For reasonably uniform samples, like the LM stalagmite, such non-uniform sampling/cutting might not be necessary. We also note that cutoffs set by the ΔARM and MAD values are problem-dependent and need to be adjusted according to the question being investigated.

BORLINA ET AL. 17 of 20

15252027, 2024, 10, Downloaded from https://agupubs

onlinelibrary.wiley.com/doi/10.1029/2024GC011594 by University Of Minnesota Lib, Wiley Online Library on [13/11/2024]. See the Terms

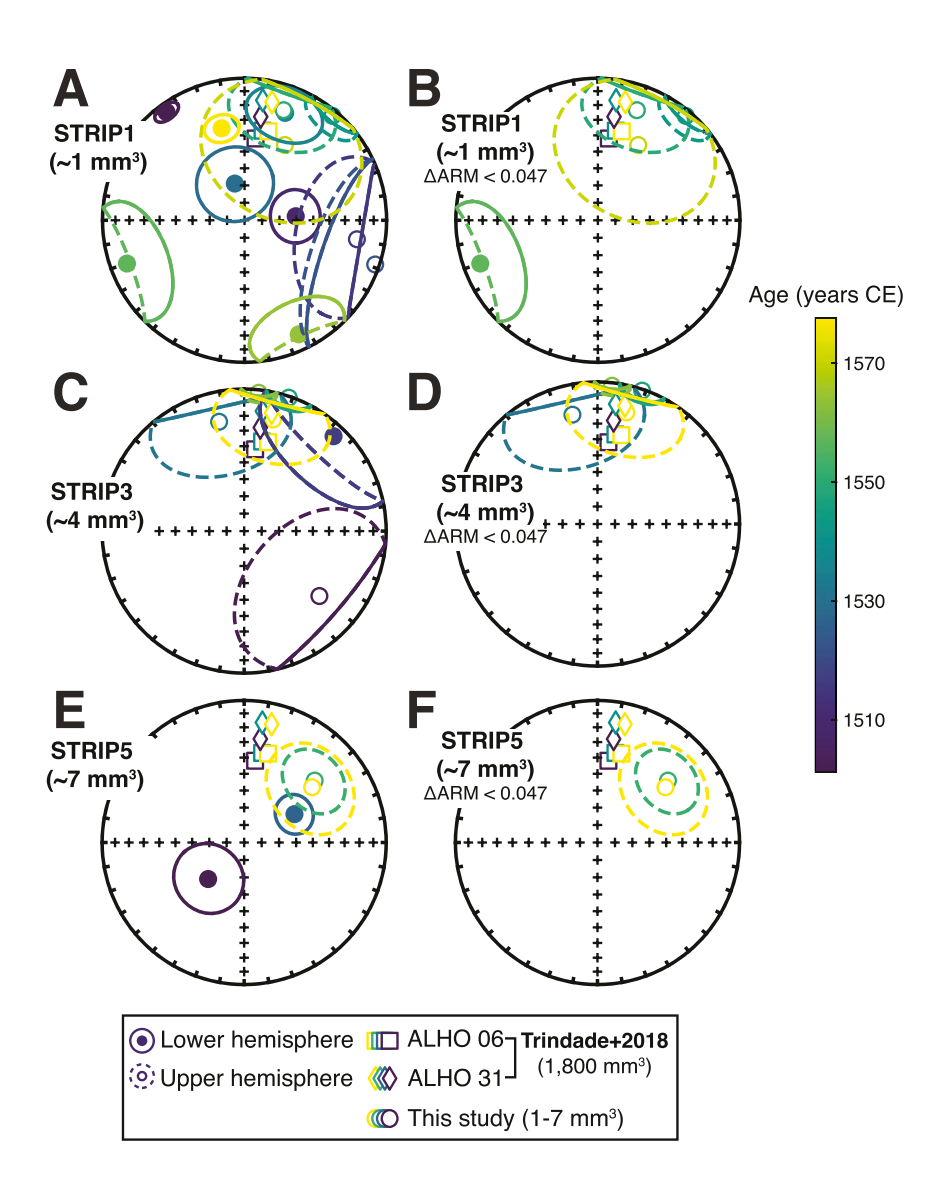


Figure 14. Comparison between high coercivity directions measured with traditional paleomagnetic techniques and superconducting quantum interference device (SQUID) microscope for Pau d'Alho (PD) samples. (a, c, e) Equal area stereographic projections showing all directions obtained from STRIP1, STRIP3 and STRIP5, respectively. (b, d, f) Equal area stereographic projections showing directions with samples that presented $\triangle ARM < 0.047$ from the same samples as (a, c, e). Results for Trindade et al. (2018) are shown as squares for ALHO06 and diamonds for ALHO31 (volumes of \sim 1,800 mm³). Circles are the SQUID microscope results from this study. Color scales indicate the ages of the samples.

5. Conclusions

We presented paleomagnetic records from three representative speleothems collected from different locations: Lapa dos Morcegos Cave (Portugal), Pau d'Alho Cave (Brazil), and Crevice Cave (USA). We report on the first paleomagnetic study of speleothems using SQUID microscopy targeting small-volume samples to test their feasibility for yielding high-temporal-resolution magnetic records. Overall, we identified that the stalagmite from Lapa dos Morcegos Cave resulted in excellent paleomagnetic data that can improve the temporal resolution of the magnetic records by at least a factor of 5 compared to measurements using traditional paleomagnetic techniques. The speleothem from Pau d'Alho contained magnetic heterogeneities that resulted in paleomagnetic data with varying quality, achieving an improvement in temporal resolution by a factor of up to 3 on average. We recommend that for speleothems with such heterogeneity, a non-uniform sampling strategy be adopted to help optimize the robustness and increase the temporal resolution of the magnetic record. Finally, we show that

BORLINA ET AL. 18 of 20

```
D
    3
                          3
                               ?&
                                          D
                                              Η
                                  8 '(:8
                                           ? ; :?
, 8 ,: , -5B, 4% J ? ';?
6 ' ? ? 3 ? ? T?T? ? ? ) 6? O ?8;;,:? ' @ ' ' C ' ' ) ' ' ' )
 ' C 788;;,%4;%2 J ?';?;-%?55;,
?G'@ (? 3 ?( (? C ?(?( ? ?8; :?'
477%B5; ;? J ?';?;; ; %; %5
6 ?? T? C ? G?6?T" &2 & ??6? ?8; :?'@
D &D :J ? 6 ,
                             6 ,
                                    -; ,;,? J ?';%57
; - 15; %
                      G?6? /" ? ? ?8; :? ' ' ' ??;%5 -4@ @
        ? ?6? & @ 6? 6 ) ' ? ?
  ? &
   @ @
 098 % % - B%; ? J ? '; ?; - KC
 ; 2,52;
```

are governed by the applicable Creative Common

```
?6 ) ' ? ? ? ? ? ( ' ?O ? ?8; -:? ' E
' ' ' ? 8: %B ? J ? ' ;? % '%4 7;?
?. ?6 ?(? 3 ? ?O &?8 757:? E ' J&
6 ( 88: %B 5? J ? ' ;?; -;; % @; 857:7;; % @
?. ? 3 ? ? 6 ?(?O .? ?8 747:? ' ' ?
L 2 ' : ? *5 5 %6 ?
                                                                                              98,4 : %5%B%5,?
     J ? ';?;%5 5;%5%;
     (?? ? ?. ?O ?8 77,:?
                                                            G
       ? ? O ? 8; -:? @'
                                                       78: 4 B54? J ? '; 2 - % K'? 474
     ' ? " ? O L " T?875;? ' ?4

0785: 5 %E5 5? J ? ';2-% K'%45 %
' ? " ? O L " T?8757?? ' 8 : ? 4

:88%, 7B, 5? J ? ';? R%, @ -E?757?);-; E

G?6? G ? ( 3 6? ? /" ? ? ? ? ? ? ? ? ? 8; -:?( @ '

? T ? ? ? '? ? '? ? 88: 4-? J ? ';?;% 4-

? T ? ? ? '? ? '? ? 88: 47? J ? ';?;% 4-

? T ? ? ? ? '? ? 88: 47? J ? ';? 5-;- %@ -@, 7%
? ? '? ? ? ? 3 (? ?8; :? @ '
? 0.8% 48 %? J ? ';? % '%-;?
        ? ? O ?8 774:?
                                                                          ( J&
                                                                             :8: 5, B;,? J ?';2-% K'?
     5,
? ? 6 ? G ' @ ( ? O @ ( ?8; 5:?
                                                                           :87: 7- B 74 ? J ? ';?; 7
     5';;4-,
2'?6 ?G'@ (? @ (?O. )) ?8; 4:?&
24 5, 6 8: %B,-? J ?';?;; ;-K; %457
(? ?8;;7:? )) ? 8: %AB%;? J ?';?; 4;;%5 ;;;%5-,
?? ??? ??? ? ? " ?.? (????8;;?& (;;
)) ') 8,B, ":? 88:4,B4,4? J ?';?; 4 ?;;?
?? &?? (????8;4:? ' @ (?.)
?? &?? (????8;5:Z ? J ?';?;; 4 ; 5-;
3@ ??6 ? @ 6?? ?? @ (?.)) ?O( ?8; :? '
C ?, 8: 47%? J ?';?; 55.
 Q 3@ C
               ? ? ? ? ? ? ? ? ? ? ? 8; %?& '
                                                                                 8 : ,;;-B,; ,? J ?';?
8: D; ;-? J ?';?;7;;%;;;-%
                                                  . ? ? 6 ) ' ? ? ?8; 5:?
       ? ?6? C ?& @ 6? ?
                                                                   8, : % 75B %; %? J ? ';?; 4% ?
5;7 74 ,
?? ??6'??O ) 6??8;;4:?
8 7: ;7;,? J ?';?; 7;;4½; 7;
L" L? L? 3 &? (? L? 3 ? ?8; :?
                                                                         ' D ?4
                                                                                  0 - B-4? J ? ';?; - K
                                    , 5
    )?; ?;?;-
';?;4% ?-;7%
```

; ;